FRICTION STIR WELDING OF OXIDE DISPERSION STRENGTHENED EUROFER STEEL–G. J. Grant and D. S. Gelles (Pacific Northwest National Laboratory),* R. J. Steel (MegaStir Technologies), and R. Lindau (FZK Karlsruhe, Germany)

OBJECTIVE

The objective of this effort is to investigate friction stir welding technology for application to oxide dispersion strengthened ferritic steels.

SUMMARY

Oxide Dispersion Strengthened Eurofer plate 6 mm in thickness in the as-received condition was successfully plasticized by friction stir welding.

PROGRESS AND STATUS

Introduction

In a previous report, friction stir welding (FSW) was demonstrated on MA957 (Fe-14Cr-1Ti-Mo-0.25Y_2O_3) a mechanically alloyed oxide dispersion strengthened ferritic steel [1]. However, a decrease in the average weld nugget hardness was observed compared to the parent material from approximately 373±21 HV to 225±22 HV. An explanation is possible based on experience with recrystallization of MA957, where it was found that hardness was considerably reduced with an accompanying large increase in dispersoid size [2]. The change was attributed to the presence of alumina stringers in the material which allowed replacement of the yttria with a coarser ruby structure. It was concluded that an alternate material was needed for future work. The present work is a continuation of that work using ODS-Eurofer. Also, it was possible to arrange for MegaStir Technologies of Provo, Utah, to perform the FSW tests. Therefore, this report summarizes recent efforts to FSW ODS-Eurofer in the as-received condition.

Experimental Procedure

The material used for this study was a plate of ODS-Eurofer measuring 12.5 x 25.0 x 0.6 cm in the as-received condition (hot cross-rolled after hipping without any subsequent heat treatment) [3]. The material was produced by Plansee to FZK specifications using Eurofer 97 (Fe-9CrWVTa) as a base material. The composition of ODS-Eurofer is given in Table 1. In order to soften the material, a tempering treatment is recommended (1100°C / 30 min/ AC + 750°C/ 2 h/ AC). The plate was provided to MegaStir Technologies, Provo, Utah, in the as-received condition. MegaStir created bead-on-plate welds using a polycrystalline cubic boron nitride tool with an embedded thermocouple shown in Fig. 1. The tool geometry uses a truncated cone surface profiled with a stepped spiral feature to promote material flow in the nugget region. Only one side of the plate was welded in order to retain enough material so that the plate could be heat treated if initial welding was unsuccessful. Metallography and electron microscopy followed standard procedures.

Table 1. Composition of the KFK ODS-Eurofer

Cr	W	V	Ta	Mn	C	Y_2O_3	Fe
9	1.1	0.2	0.14	0.4	0.08	0.3	balance

*Pacific Northwest National Laboratory (PNNL) is operated for the U.S. Department of Energy by Battelle Memorial Institute under contract DE-AC06-76RLO-1830.

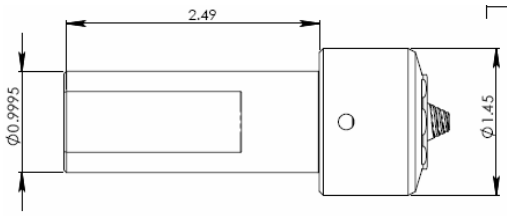

Fig. 1. Design of the BN tool bit used for FSW, dimensions in inches.

Results

Bead-on-plate friction stir welds were successfully performed by MegaStir on as-received ODS-Eurofer plate. The first weld was performed at a spindle rotation of 150 rpm and a travel speed of 2.5 cm/min. These conditions resulted in an unstable (cold) weld so the spindle speed was increased to 300 rpm. Welding parameters are included in Table 2. Weld process parameter development was limited to two conditions due to the nature of this exploratory study. Weld 2 at 300 rpm showed excessive flash on the surface so it is likely that this weld condition was too hot for an appropriate weld in this material. The top surface and root zone of the as-welded plate sections are shown in Fig. 2. In addition, the tool used for this study was not optimized for this material thickness. The pin was ~ 0.5 mm too long causing a root side defect with a small amount of backing plate material (mild steel with mill scale) incorporated in the stir zone. Note that weld pass #2 was longer and that part of the weld is not shown. Figure 2 illustrates the root side surface showing the penetration defect.

Table 2. Weld process parameters

Weld No	Weld Speed (cm/min)	Spindle speed (rpm)	Condition	Peak Temperature (°C)
1	2.5	150	No preheating	758
2	2.5	300	No preheating	915

Weld 2 was sectioned approximately at the bottom of Fig. 2b, and hardness traverses were taken across the weld and through the weld thickness over the advancing side of the weld on an as-polished surface, as shown in Fig. 3. Figure 3 includes an optical metallogram, inset, showing the advancing half of the weld with the central nugget on the right and with all hardness indentations visible. From Fig. 3, it can be shown that the hardness is reduced from ~ 350 DPH to ~ 300 DPH in the heat affected zone, but jumps to ~ 450 DPH in the thermomechanically affected zone (TMAZ), dropping to ~ 400 DPH in the recrystallized nugget. Significant hardening occurs in both the TMAZ and the nugget regions.

The weld microstructure is shown in greater detail in Fig. 4. The structure has been revealed using Villela's etch, so that the TMAZ shows greater structure than in the inset of Fig. 3. Figure 4 shows the FSW retreating side on the left and the advancing side on the right. A defect is apparent on the lower part of the retreating side at the nugget interface. This region is shown as a mosaic in greater detail in Fig. 5 for an as-polished surface. Three cracks are present as well as several seams of stirred-in foreign matter. It is anticipated that this defect is a result of the tool bit penetrating the supporting mild steel plate and stirring in the mill scale on the support plate.

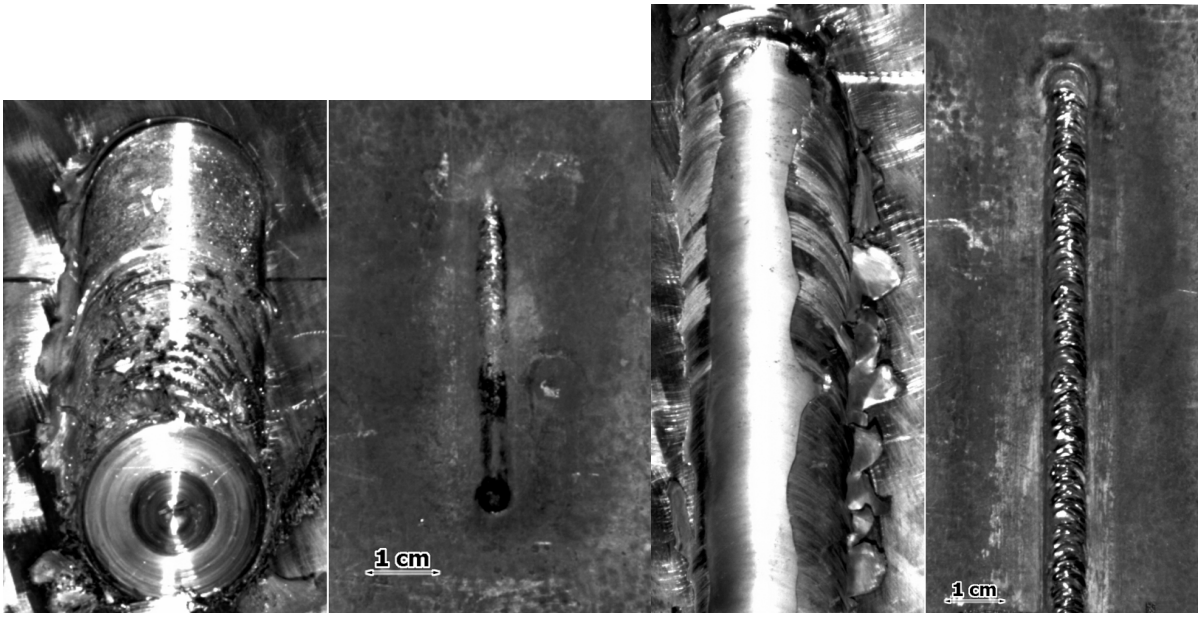

Fig. 2. Top and bottom surfaces of FSW passes 1 and 2 on ODS-Eurofer in the as-received condition.

The microstructure of the nugget region was examined by electron microscopy and found to be highly dislocated, with only coarse precipitates, whereas the as-received structure contained much finer precipitate structure. An example of the structure in the nugget of FSW #2 is given in Fig. 6. Many of the particles are 50 nm in diameter and several are much larger.

Comparison between the FSW and as-received structures is provided in Figs. 7 and 8. Figure 7 shows the nugget structure and Fig. 8 gives the as-received structure, both with composition maps, but at very different magnifications. The composition maps allow comparison of Y and Ta distributions with a map using a background window included to provide a relative measure of thickness. Figure 7 demonstrates that Ta is more finely distributed but often in association with the large Y particles in the FSW. In comparison, in the as-received condition, Y and Ta particles are separated and more finely distributed. (At the upper left, two particles are almost superimposed.)

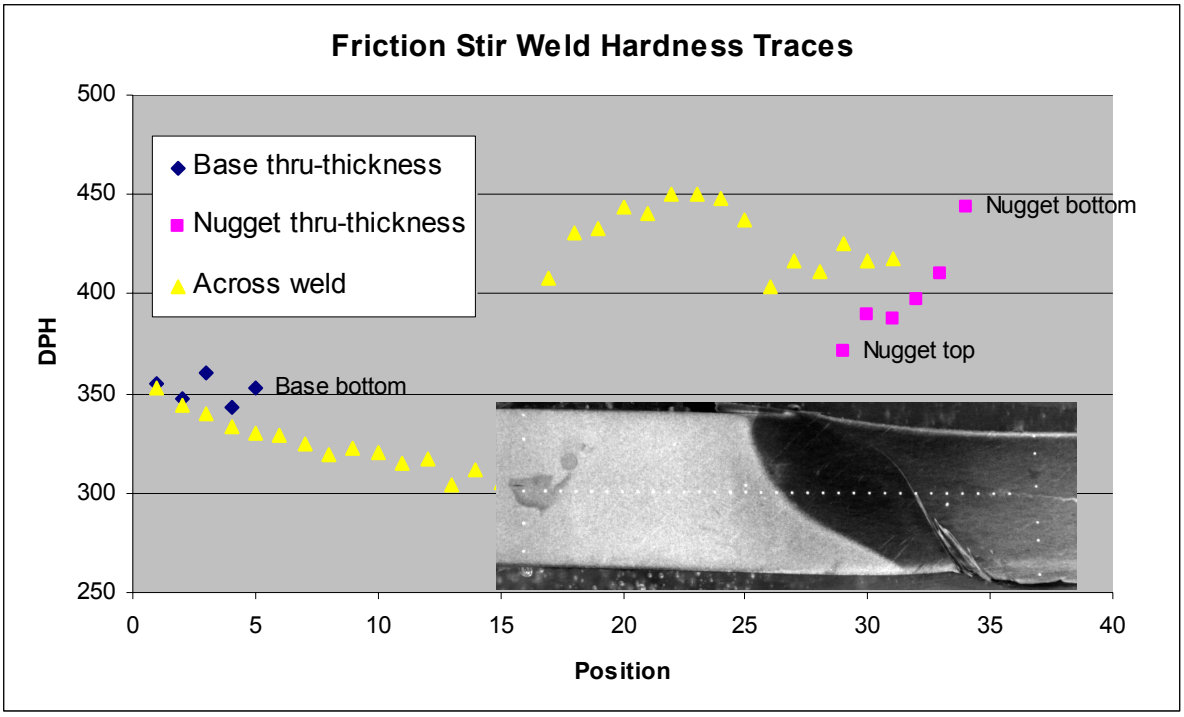

Fig. 3. Diamond Pyramid hardness (DPH) as a function of position for FSW 2. A metallogram is inset which shows the hardness locations from left to right for the 6-mm thick plate.

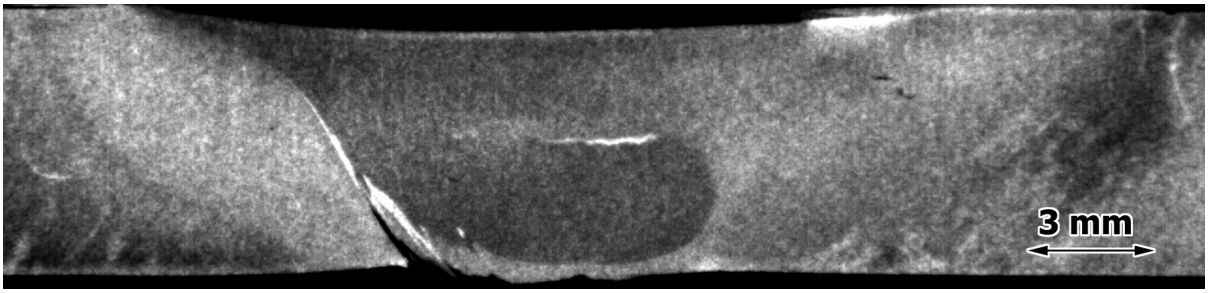

Fig. 4. Etched cross-section of FSW #2.

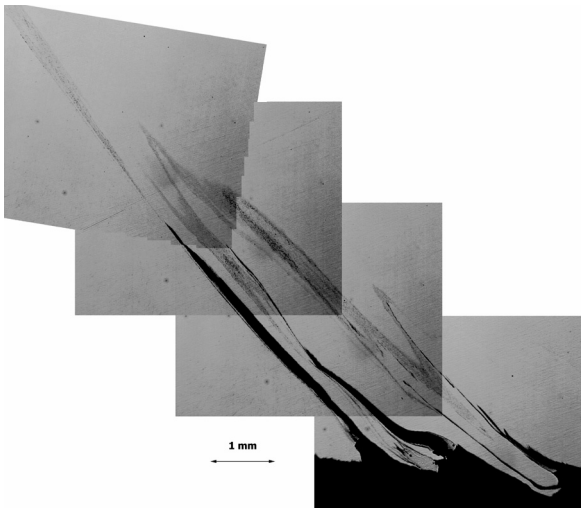

Fig. 5. Higher magnification example of the weld defect in FSW #2.

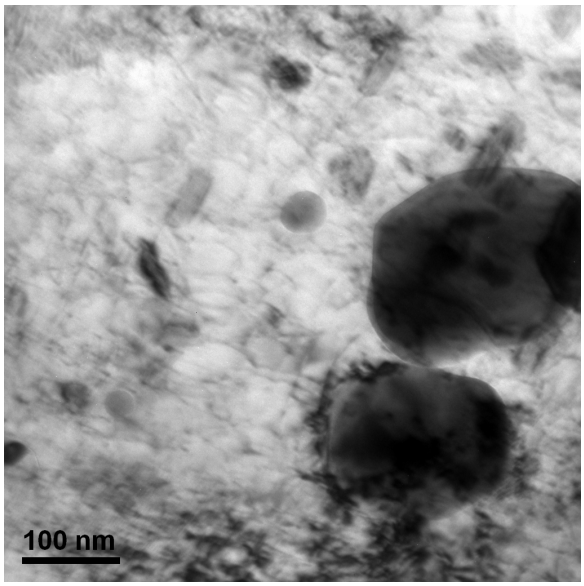

Fig. 6. Precipitate and dislocation structure in the nugget of FSW #2.

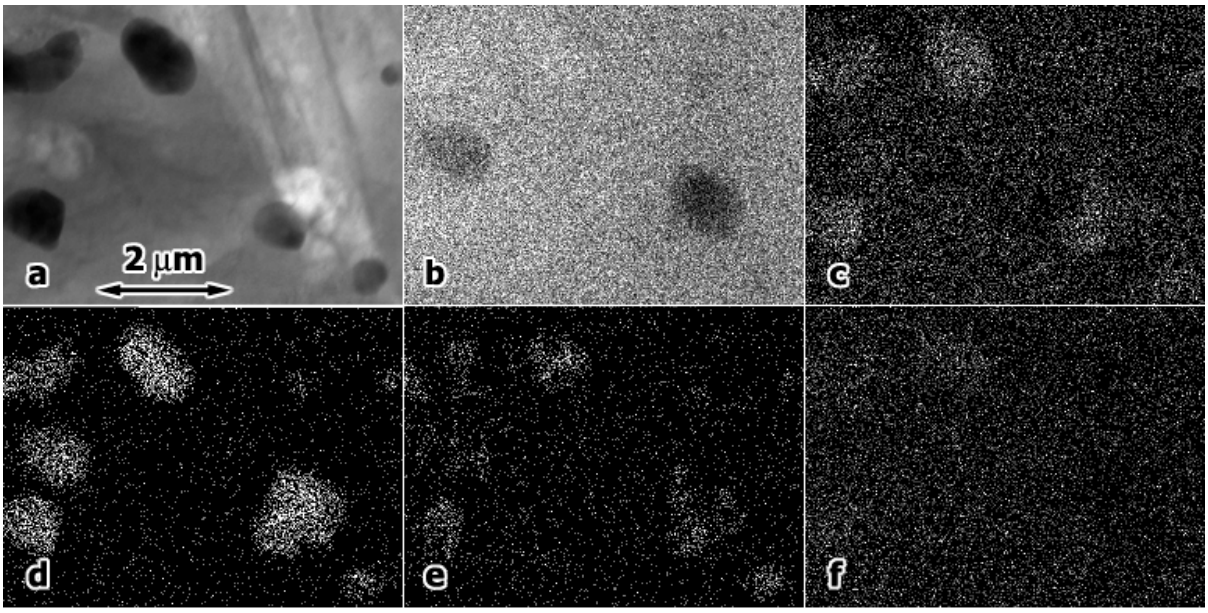

Fig. 7. Precipitate particles in the nugget of FSW #2 showing a) the area of interest, composition maps for b) Fe $K_{\alpha 1}$, c) O $K_{\alpha 1}$, d) Y $K_{\alpha 1}$, and e) Ta $L_{\alpha 1}$, and f) an x-ray background map showing relative thickness.

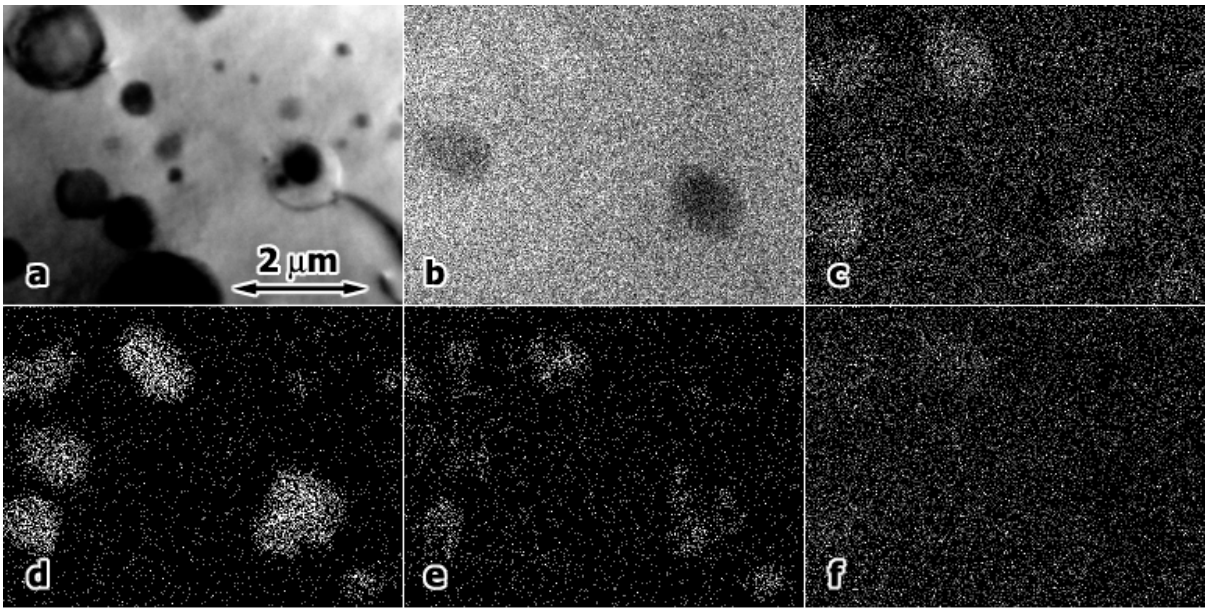

Fig. 8. Precipitate particles in as-received ODS-Eurofer showing a) the area of interest, composition maps for b) Fe $K_{\alpha 1}$, c) O $K_{\alpha 1}$, d) Y $K_{\alpha 1}$, and e) Ta $L_{\alpha 1}$, and f) an x-ray background map showing relative thickness.

Discussion

The as-received condition of ODS-Eurofer includes particles as small as 5 nm, and most are Y_2O_3, but several are TaO_2, whereas in the nugget of FSW #2 particles are much coarser, generally larger than 50 nm and often containing Y_2O_3, with embedded discrete TaO_2 particles. Significant coarsening of the dispersoid appears to have occurred during FSW, with coalescence of Y_2O_3 and TaO_2 phases. The particle distributions cannot account for the hardening observed in the nugget. As the nugget region generally undergoes dynamic recrystallization, the high dislocation density observed likely demonstrates that a martensite transformation occurred on cooling, which probably provides explanation for observed hardening in the nugget.

The cause of the particle coarsening is worthy of speculation. Peak temperatures recorded at the tool bit during FSW were fairly low, 758 and 916°C for welds 1 and 2, respectively, and the weld times were short, 4 and 6 minutes. BN has good heat transfer properties, so it is anticipated that the temperature was not much hotter under the tool bit. Therefore, it is hard to envision that bulk diffusion would promote much coarsening, given the operating temperature and time at temperature. For comparison, Alinger and Odette predict that effective coarsening of the dispersoid will occur at 1000°C only after 10^4 h [4]. It has been shown that in MA957, dynamic recrystallization is required to cause dissolution of the dispersoid, to be replaced by a ruby compound [2]. It therefore seems likely that the dynamic recrystallization that occurs during FSW may be responsible for the large coarsening observed. Not only does grain boundary diffusion play a role, but the exothermic response due to the annihilation of the energy stored in the dislocation structure and the opportunity for pipe diffusion should enhance diffusion processes. Nonetheless, transfer of that much matter by coarsening is unexpected, and particle accumulation at moving boundaries, transference over large distances and coalescence may be primarily responsible for the coarsening that was observed. We may be able to shed further light on the kinetics of this process by examining coarsening behavior in the nugget of FSW #1, which reached a temperature ~ 150°C lower.

Conclusions

The ODS-Eurofer alloy can be successfully plasticized by FSW.

Future Work

The effort will be continued as opportunities become available.

References

[1] S. M. Howard, B. K. Jasthi, W. J. Arbegast, G. J. Grant, S. Koduri, D. R. Herling, and D. S. Gelles, DOE/ER-0313/37 (2004) 55.
[2] M. L. Hamilton, D. S. Gelles, R. J. Lobsinger, M. M. Paxton, and W. F. Brown, Fabrication Technology for ODS Alloy MA957, PNL-13165 (2000) 10.
[3] R. Lindau, A. Möslang, A. Alamo, C. Cayron, G. Filacchioni, R. Schäublin, and E. Diegele, presented at the International Symposium on Application of Nano-particle Dispersion Strengthened Steels to Advanced Nuclear Power Plant, December 6–7, 2003, Kyoto, Japan.
[4] M. J. Alinger and G. R. Odette, DOE/ER-0313/37 (2004) 61.